Synthesis of radical-bridged lanthanide heterobimetallic complexes

Samuel J. Horsewill,* Tajrian Chowdhury, Anna G. Bailey, William J. Peveler, Gordon J. Hedley, Claire Wilson and Joy H. Farnaby*

School of Chemistry, Joseph Black Building, University of Glasgow, University Avenue, Glasgow, G12 8QQ.

** Corresponding authors: SJH, sh3228@bath.ac.uk; JHF, Joy.Farnaby@glasgow.ac.uk.*

Summary paragraph

Heteromultimetallic lanthanide (Ln) molecules are used in sensing and imaging,[1-3] and have recently demonstrated Ln-to-Ln energy transfer[4-8] and potential as quantum logic processors.[9-11] However, the selective synthesis of molecular Ln heteromultimetallics is challenging, limiting further investigation of their properties and applications. For example, redox-active ligands mediate *f*-block reactivity with small molecules[12-15] and have applications in molecular magnetics[16, 17] in homometallic Ln systems, yet have not been incorporated into heteromultimetallic complexes. Herein, we utilise the chemically distinct binding sites and redox chemistry of 1,10-phenanthroline-5,6-dione (pd) to synthesise radical-bridged Ln heterobimetallic complexes. In a stepwise, modular, and extendable synthesis, we tailor the ancillary ligand environment to generate selectivity within the non-directional ionic bonding regime typical for Ln ions. The selectivity of binding for two lanthanide combinations with different ionic radius ratios is demonstrated by solution-state spectroscopy (NMR, UV-vis, photoluminescence) spectroscopies, and confirmed in the solid-state by crystallographic determination of the molecular structures. In preliminary photoluminescence studies, we observe complex, selective energy transfer unusually involving the radical ligand. Our synthetic strategy enables any pair of lanthanide ions to be combined and will be widely applicable in the preparation of heteromultimetallic complexes of otherwise non-selective metal ions.

Introduction

Lanthanide ions (Ln) possess unique photophysical and magnetic properties, finding application in magnetic[16-20] and optical technologies, both at bulk and molecular scales.[21-24] While bulk systems offer scalability and high stability, molecular systems allow exquisite structural and electronic control, leading to extraordinarily effective molecules. Molecular design has produced record breaking molecular magnets and highly emissive complexes.[19-21] Combining multiple, different Ln in a molecular species is desirable to design multimetallic systems for sensing, optics, and quantum information science.[1-11, 25] However, the ionic bonding of Ln and their resultant chemical similarity makes selective synthesis of heteromultimetallic molecules challenging.

Strategies that have been used to overcome the challenges of Ln heterobimetallic synthesis can be grouped into two broad categories: thermodynamic and kinetic control. Thermodynamic control involves ligands which use variation in ionic radius across the period to statistically assemble selective heterometallic complexes. Ln with large differences in ionic radius therefore selectively coordinate at different ligand sites. Early studies using this approach achieved high selectivity,[26, 27] and complete selectivity has been achieved in paddlewheel-like multimetallic systems (**Figure 1a**).[9, 10]

Kinetic control uses ligands which form kinetically inert complexes under reaction conditions, with high binding constants (typically $K > 10^{12}$) so that redistribution is inaccessible.[28] Individual kinetically inert complexes are then linked to construct multimetallic architectures (**Figure 1b**). This approach was first used to assemble stacked

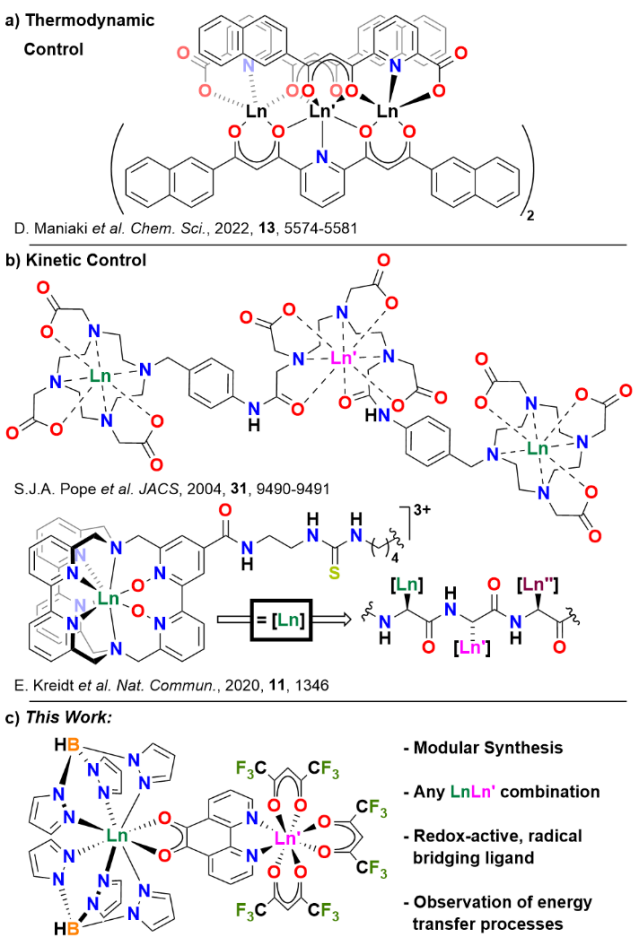

Figure 1: Examples of heterometallic lanthanide complexes prepared *via* **(a)** thermodynamic control;[10] **(b)** kinetic control;[2, 4] or **(c)** combined thermodynamic selectivity of kinetically inert moieties to an asymmetric bridging ligand (this work).

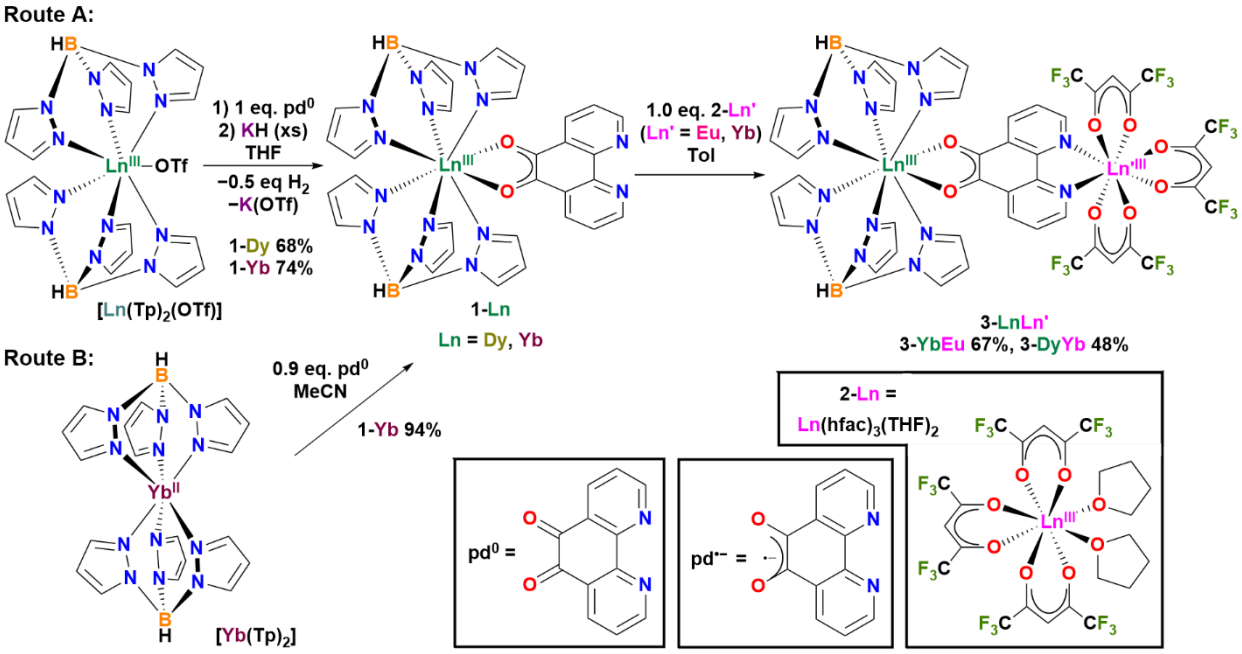

Scheme 1: Two synthetic routes to **1-Ln** (Ln = Dy, Yb) and the synthesis of heterobimetallic complexes **3-YbEu** and **3-DyYb**.

porphyrin sandwich complexes,[29] but has also been used for the synthesis of cyclic amine carboxylate heteromultimetallic complexes.[4, 5] Recently, stepwise synthesis of peptides with immobilised Ln-containing side groups has been shown to provide flexible access to multimetallic complexes with higher nuclearities, and with the potential for further scalability.[1, 2]

While successful for the preparation of a range of heterometallic complexes, these strategies inherently limit Ln combinations and/or the bridging and ancillary ligands they incorporate. Targeting specific properties in bridging ligands can be particularly challenging. As a result, despite the importance of non-innocent ligands in *f*-block reactivity,[12-15] interest in radical ligands for molecular magnetism,[16, 17] and applications of multi-spin systems in spintronics, Ln heteromultimetallic complexes containing redox-active bridging ligands have never previously been reported. To address this, we set out to develop a flexible strategy for heterometallic complex synthesis that would allow the introduction of new types of bridging ligand between non-selective metal ions such as lanthanides. In this study, we use a redox-active radical bridge as a template. Our strategy combines the principles of the two approaches previously used for Ln heterobimetallics: individually kinetically inert Ln precursor complexes are designed using ancillary ligands to exhibit thermodynamic selectivity to different binding sites of a bridging ligand.

Our group and others have reported selective coordination of Ln to the asymmetric redox-active ligand 1,10-phenanthroline-5,6-dione (pd, **Scheme 1**). The pd ligand has three different accessible oxidation states, where sequential reduction of the neutral pd ligand results in electronic structure changes at the *O,O'* site (pd^0, dione; pd$^{\bullet-}$, semiquinone; and pd^{2-}, catecholate). Conveniently, Ln *tris*-*β*-diketonate moieties coordinate selectively at the diimine *N,N'*-binding site in all three oxidation states of the ligand.[30-33] For this work, we chose to focus on pd$^{\bullet-}$ to take advantage of the selectivity of the [Ln(Tp)$_2$]$^+$ moiety (Tp = hydrotris(1-pyrazolyl)borate) to anionic bidentate *O*-donor ligands (*e.g.* semiquinones, *β*-diketonates).[34-38] We expected that [Ln(Tp)$_2$]$^+$ should therefore target the *O,O'*-binding site of pd$^{\bullet-}$ over the *N,N'* site. In combination with the established *N,N'* selectivity of *tris*-diketonates, this modular route allows us to construct well-defined heterobimetallic complexes, the first of which to incorporate a radical bridging ligand. We study two Ln pairings with opposite radius ratios and show how the strategy is applicable for any combination. We establish the selectivity of the binding for the two chosen lanthanide pairings in the solution state by NMR, UV-Vis-NIR and photoluminescence (PL) spectroscopies, as well as by X-ray crystallography. Our preliminary investigation into the PL of the heterobimetallic revealed complex energy transfer (ET) pathways including selectivity in and participation of the radical bridging ligand in sensitisation.

Results and Discussion

Synthesis

We demonstrate here two routes to synthesise the semiquinone complex [Ln(Tp)$_2$(*O,O'*-pd)] **1-Ln** (**Scheme 1**). We have previously shown that potassium hydride (KH) is competent for single-electron reduction of pd^0,[31] and yet does not reduce Ln^{3+} in [Ln(Tp)$_2$]$^+$ complexes to Ln^{2+}. Thus, [Ln(Tp)$_2$(OTf)] (Ln = Dy, Yb; OTf = trifluoromethylsulfonate) was added to a yellow suspension of pd in THF, followed

by addition of excess KH, a deep red-orange solution resulted from which **1-Ln** (Ln = Yb, 74%; Dy, 68%) were isolated as brick-red solids (Route A). The solubility of **1-Ln** is high in polar solvents and low in non-polar aromatic solvents.

Alternatively, for Ln = Yb, a different route was also accessible. In MeCN, addition of the divalent ytterbium (Yb^{2+}) reagent [Yb(Tp)$_2$] as a one-electron donor reduced pd^0 to $pd^{\bullet-}$ directly providing trivalent (Yb^{3+}) **1-Yb**, which was isolated as a brick-red solid in near-quantitative yield (94%) (Route B). While higher-yielding, this route is not feasible for the majority of Ln, as [Ln(Tp)$_2$] is not stable for many Ln^{2+} (including Dy), and [Eu(Tp)$_2$] is insufficiently reducing to react.[39]

Having achieved selective *O,O'*-coordination in **1-Ln**, our attention turned to preparing the heterobimetallic complexes. The reaction of anhydrous Ln(OTf)$_3$ with 3 eq. K(hfac) in THF produces the *N,N'*-selective precursor [Ln(hfac)$_3$(THF)$_2$] **2-Ln** in excellent yields (Ln = Eu, Yb; see ESI **Section A2**). A solution of **2-Ln** was added dropwise to **1-Ln** in toluene (**Scheme 1**). A colour change from red-orange to a plum-red solution was observed upon mixing, and after workup [(Tp)$_2$Ln(*O,O'*-*N,N'*-pd)Ln'(hfac)$_3$] (**3-YbEu**: Ln = Yb, Ln' = Eu, 67%; **3-DyYb**: Ln = Dy, Ln' = Yb, 48%) was acquired as maroon solids. To avoid ligand redistribution, the reaction was stopped after 15 minutes. Elemental analysis confirmed the expected formulation of **3-YbEu** and **3-DyYb**. **3-LnLn'** are soluble in aromatic solvents and moderately so in aliphatic solvents.

We confirmed the stability of **3-LnLn'** in solution by tracking formation of redistribution products by NMR (see ESI **Table S2** for details). Despite the short reaction times required, after isolation **3-YbEu** and **3-DyYb** were each stable in non-polar solvents for up to 24 h (with a final redistribution of only *ca.* 15% *after several days*). All spectra discussed herein were nevertheless recorded immediately after sample preparation. In the solid state, **3-LnLn'** were stable for at least three months under inert atmosphere. However, rapid redistribution was observed in polar solvents, producing [Ln(Tp)$_2$(hfac)] and other byproducts. Polar solvents were therefore not used in the spectroscopic analysis of **3-LnLn'**.

Structural characterisation

The ^{1}H, ^{19}F and ^{11}B NMR spectra of **1-Ln**, **3-YbEu** and **3-DyYb** as recorded in d_6-benzene exhibit significant pseudo-contact shifts (PCS) from the anisotropic paramagnetic Ln metal centres, causing the resonances to move significantly outside the typical ranges for the ligands. Despite the complex system with up to three different paramagnets, the spectra are fully assignable (see ESI **Table S1**). In fact, the PCS from the Tp-bound paramagnetic Ln^{3+} significantly aid assignment of the data.

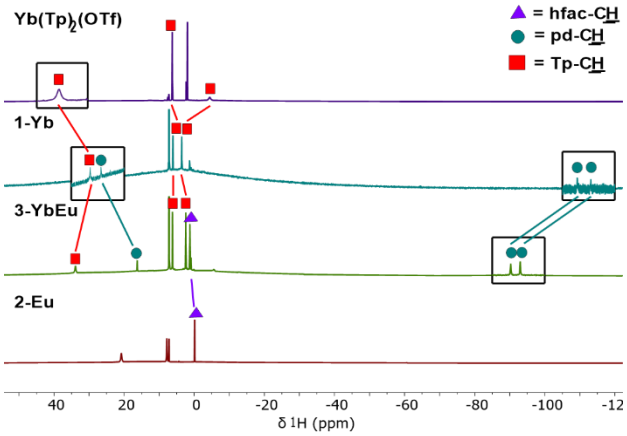

Figure 2: ^{1}H NMR spectra of Yb(Tp)$_2$(OTf) (d_3-MeCN), **1-Yb** (d_3-MeCN), **3-YbEu** (d_6-benzene) and **2-Eu** (d_6-benzene), showing the correlation of the chemical shifts of hfac-C**H** (purple triangles), pd-C**H** (teal circles) and Tp-C**H** (red squares). Expansions are provided (black boxes) with increased intensity for clarity.

We have previously reported that $[CoCp_2]^+[pd]^{\bullet-}$ did not exhibit ^{1}H resonances which could be assigned to $pd^{\bullet-}$.[31] Surprisingly, however, the ^{1}H NMR spectra of **1-Ln** and **3-LnLn'** exhibit resonances which are assigned to ^{1}H environments of the $pd^{\bullet-}$ ligands. We attribute this to the coordination of Ln^{3+} in the *O,O'* binding site of $pd^{\bullet-}$. The ^{1}H NMR resonances in **1-Ln** were assigned to the $pd^{\bullet-}$ or Tp ligands by relative integration. Shown in **Figure 2** are the ^{1}H NMR spectra of Yb(Tp)$_2$(OTf), **1-Yb**, **3-YbEu** and **2-Ln**, which highlights the evolution of the resonances assigned to the different ligands over time. The PCS contribution to the Tp-C**H** resonances (red squares) in Yb(Tp)$_2$(OTf) is moderated by the coordination of $pd^{\bullet-}$ in **1-Yb**. The coordination of the second Ln^{3+} in **3-YbEu** further moderates the overall chemical shifts of the hfac (purple triangles), pd (teal circles) and Tp (red squares) resonances from those in **1-Yb** and **2-Eu**. However, the number of resonances, relative integrations, and relative magnitudes of the PCS shift do not change, facilitating assignment of the resonances (for **3-DyYb** see ESI **Figure S33**).

Single crystals of **1-Ln** were obtained by crystallisation from MeCN solutions with antisolvent at −35 °C, and of **3-LnLn'** by cooling saturated solutions to −35 °C. The solid-state molecular structures of **1-Dy** and **3-YbEu** are shown in **Figure 3** (see ESI Section B5 for **1-Yb**, **2-Eu**, **3-DyYb**). As expected, **1-Dy** and **1-Yb** each show the metal bound in the *O,O'*-binding site of the $pd^{\bullet-}$ ligand with axially coordinated κ^3-Tp ligands. The molecular structure of **3-LnLn'** shows Yb or Dy bound in the *O,O'*-binding site with Eu or Yb bound in the *N,N'*-binding site, while retaining the expected ancillary ligand environment from the stepwise synthesis, evidencing the selective coordination. We note that refinement of the molecular structure revealed that the displacement parameters in **3-DyYb**, (U_{eq}) were more consistent with the lanthanide ions occupying the opposite

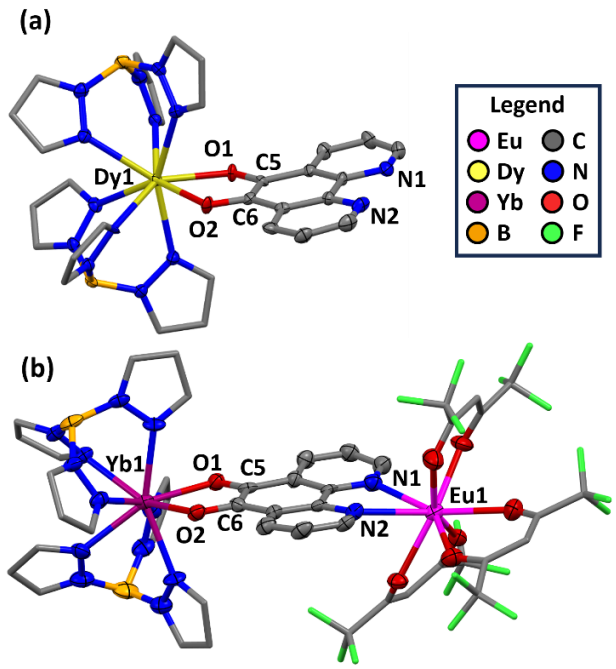

Figure 3: Solid-state molecular structures of (a) **1-Dy** and (b) **3-YbEu**. H atoms and lattice solvent molecules omitted, and C and F atoms of Tp and hfac displayed as sticks only for clarity. Thermal ellipsoids drawn at 50% probability. Bond metrics can be found in the ESI **Table S4**.

positions to those expected (*i.e.* $[(Tp)_2Yb(O,O'\text{-}N,N'\text{-}pd)Dy(hfac)_3]$). However, considering all other parameters are more consistent with the **3-DyYb** structure, as are the spectroscopic data of the single crystals themselves (*eg.* NMR, PL), we are confident the crystals obtained are best described as such (see ESI, **Section B5** for further details).

The bond distances of the *O,O'*-binding site of pd are dependent on the ligand oxidation state (O1-C5-C6-O2 in **Figure 3**). The C–C and C–O bond distances in **1-Ln** and **3-YbEu** are intermediate between those observed in lanthanide complexes of pd^0 and pd^{2-}, and are consistent with uncoordinated $pd^{\bullet-}$ in $[CoCp_2]^+[pd]^{\bullet-}$ (see SI, **Table S4**), confirming our assignment of the ligand oxidation state as $pd^{\bullet-}$ in both **1-Ln** and **3-LnLn'**.[30, 31, 40] Solid-state structural data are tabulated in the ESI (**Table S4**) along with additional crystallographic information including the molecular structures of **2-Eu** and **3-DyYb** (ESI **Section B5**).

Electronic absorption and emission

The absorption spectra of **1-Ln** recorded in MeCN or toluene are very similar. In MeCN, a single absorption feature is observed in the UV region, assigned to π-π* transitions of pd (**1-Yb**, λ_{max} = 273 nm, ε = 3.1×10^4 M^{-1} cm^{-1}, **Figure 4a**; **1-Dy**, λ_{max} = 272 nm, ε = 2.3×10^4 M^{-1} cm^{-1}, ESI **Figure S41**). Three absorption maxima are observed in the visible region (>380 nm) (**1-Yb**, λ_{max} = 394, 474, 532 nm; **1-Dy**, 394, 474, 528 nm). The most intense feature for each is the absorption at λ_{max} = 474 nm, which has molar extinction coefficients (**1-Yb**, ε = 3879 M^{-1} cm^{-1}; **1-Dy**, ε = 3120 M^{-1} cm^{-1}) which are consistent with visible absorptions we have previously assigned to the $D_0 \rightarrow D_1$ transition of $[CoCp_2]^+[pd]^{\bullet-}$ (ε = 3230, 3830 M^{-1} cm^{-1}).[31]

The visible absorption spectra of **3-YbEu** and **3-DyYb** recorded in toluene show less intense and defined features compared to **1-Ln**. A single broad absorption feature is evident in the visible region with λ_{max} = 492 nm (**3-YbEu**, ε = 3023 M^{-1} cm^{-1}, **Figure 4b**; **3-DyYb**, ε = 930 M^{-1} cm^{-1}, ESI **Figure S46**), similar in energy to the visible absorptions of **1-Ln**. Strong absorptions were also evident in the UV region, however due to the incompatibility of **3-LnLn'** with MeCN, absorptions below 300 nm were not quantified.

Organic radicals have gained some attention lately for their photoluminescence,[41, 42] but examples of emission from organic radical-containing compounds are scarce due to rapid excited state quenching. Nevertheless, upon excitation either in the UV or visible, **1-Yb** displayed characteristic NIR emission from Yb^{3+} (λ_{max} = 975 nm, **Figure 4a**). Interestingly, the emission intensity was broadly proportional to molar extinction co-efficient at each of the wavelengths used, despite assignment of the absorptions in the visible region to excitation of $pd^{\bullet-}$,[31] which is coordinated to Yb^{3+} *via* the radical semiquinone *O,O'* binding site. Excitation of **1-Dy**, meanwhile, resulted in negligible emission from Dy^{3+}, which was only observed upon irradiation with UV light (ESI **Figure S49, S50**). Presumably, there is no efficient ET pathway due to the similarity in excited state energies between $pd^{\bullet-}$ and Dy^{3+}. In contrast, excitation of the π-π* transition of the hfac ligand in $[Dy(Tp)_2(hfac)]$ elicited bright emission from Dy^{3+} (see ESI **Figure S56**).

The PL spectra of **3-LnLn'** were recorded with a range of excitation wavelengths targeting the absorptions of the different ligands (hfac, λ_{Ex} = 317 nm; $pd^{\bullet-}$, λ_{Ex} = 474, 526 nm). Note that from the absorption spectra of **1-Ln**, pd also exhibits some absorbance near 317 nm, albeit at lower intensity (see **Figure 4a**, **1-Yb** *vs.* **2-Eu**). As a control, **2-Ln** afforded typical Ln^{3+} emission spectra upon excitation of the hfac ligands (**2-Eu**, **Figure 4a**; **2-Yb**, ESI **Figure S51**). As shown in **Figure 4b**, excitation *via* the hfac ligand in **3-YbEu** resulted in emission from Eu^{3+} (λ = 575-700 nm) and to a lesser extent Yb^{3+} (λ = 975-1050 nm). Contrastingly, direct excitation of $pd^{\bullet-}$ in the visible region produced NIR emission from Yb^{3+} only. In **3-DyYb**, (see ESI, **Figure S54**) excitation of the hfac ligand resulted predominantly in Yb^{3+} emission, along with somewhat lower levels of emission from Dy^{3+} (λ = 475-750 nm). Excitation of $pd^{\bullet-}$ however resulted only in emission from Yb^{3+}, in line with our observations of **1-Dy**. As in the case of **1-Ln**, excitation of the radical $pd^{\bullet-}$ ligand in **3-LnLn'** here unusually results in emission from Ln^{3+} ions.

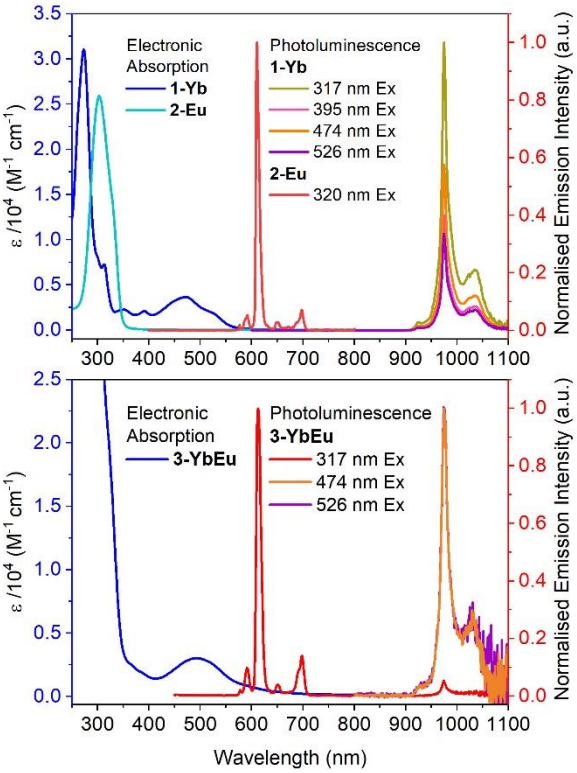

Figure 4: (a) *LHS*, overlay of electronic absorption spectra of **1-Yb** and **2-Eu** in MeCN; and *RHS*, overlay of emission spectra of **1-Yb** in toluene and **2-Eu** in MeCN (emission spectra of **1-Yb** normalised to the highest intensity); **(b)** *LHS*, electronic absorption spectra of **3-YbEu** in toluene; and *RHS*, overlay of emission spectra of **3-YbEu** in toluene (emission spectra individually normalised)

The Yb^{3+} emission spectra of *O,O′*-coordinated **1-Yb** and **3-YbEu** or $[Yb(Tp)_2(hfac)]$ (**Figure 4a**, ESI **Figures S48**, **S57**) each exhibit two maxima, one of which has significantly greater intensity (λ_{max} = 975 (intense), 1030 nm). In contrast, **3-DyYb** gives three emission maxima, each of similar intensity (λ_{max} = 975, 1005, 1030 nm, ESI **Figure S54**). We attribute this change in profile to the greater ligand field effect experienced by $Yb(hfac)_3$ in the *N,N′* diimine site of pd when compared to $[Yb(Tp)_2]^+$ in the *O,O′* site, which alters the Stark splitting of Yb^{3+} excited state sublevels. These differences are only possible with selective coordination of Yb^{3+} to either the *O,O′* or the *N,N′* binding site. Notably, three emission maxima of similar intensities were also observed from $[Yb(hfac)_3(N,N'\text{-}pd^0)]$.[43]

To understand the differences in excitation patterns between **3-YbEu** and **3-DyYb**, it is informative to consider the possible ET pathways as shown in **Figure 5**. Excitation of the hfac ligands (λ_{Ex} = 317 nm) always results in emission from the lanthanide coordinated to hfac, bound in the *N,N′* binding site of the pd ligand (pathway **I** in **Figure 5a** and **5b**), as well as ET to the Ln^{3+} bound in the *O,O′* binding site. Alternatively, excitation of the $pd^{\bullet-}$ ligand has different results depending on Ln coordinated. In **3-YbEu**, energy

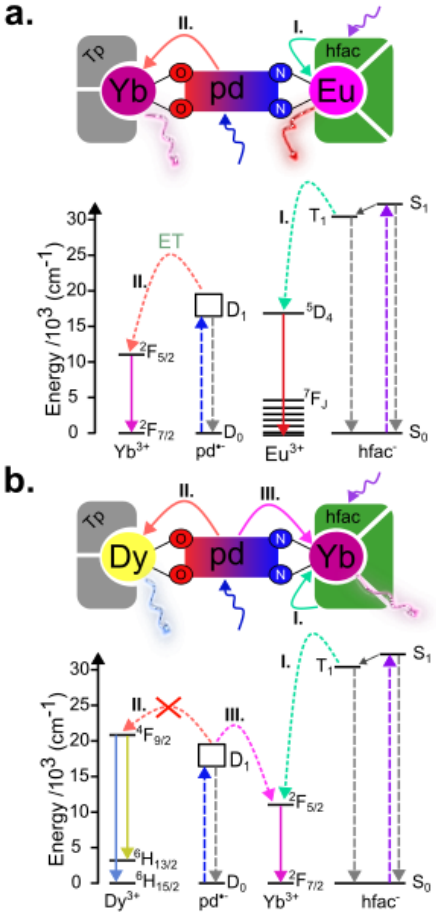

Figure 5: Energy level diagrams with graphical representations of ET and BET pathways in **(a) 3-YbEu** and **(b) 3-DyYb**. Key for energy level diagrams: ET, curved dashed arrows; Excitation, coloured dashed arrows; non-radiative decay, grey dashed arrows; and radiative decay, coloured solid arrows.

transfer to Yb^{3+} in the *O,O′* binding site occurs (pathway **II** in **Figure 5a**). However, there is no efficient route for energy transfer to Dy^{3+} from $pd^{\bullet-}$, making this pathway unviable in **3-DyYb**. Instead, in **3-DyYb** excitation of $pd^{\bullet-}$ results in energy transfer to Yb^{3+} in the *N,N′* binding site (pathway **III** in **Figure 5b**). These complex and directional energy transfer pathways provide further evidence for selective coordination to *N,N′* and *O,O′* coordination sites.

We note that in both **3-YbEu** and **3-DyYb**, while excitation of the hfac ligands primarily results in emission from the Ln^{3+} coordinated to the hfac ligands in the *N,N′* binding site (ET pathway **I**), minor emission contributions were always observed from the Ln^{3+} coordinated to the *O,O′* binding site. This is consistent with a less efficient, long-range ET pathway (*eg.* Förster Resonance ET) operating in parallel with short-range pathway **I**. Alternatively, it is possible that this arises from excitation of a high-energy transition of $pd^{\bullet-}$, which features some absorption in the same region as the hfac ligands. However, population of the lower-lying excited states of $pd^{\bullet-}$ (visible excitation) does not result in emission from Dy^{3+} in **3-DyYb**, whereas higher energy (UV excitation)

does. Thus, *either* ET may occur from a higher excited state of pd accessed by UV irradiation (*anti*-Kasha type behaviour) *or* long-range ET from distant hfac ligands is operative and competing with pathway **I**. Our current data does not distinguish these pathways.

Conclusion

In this study, we have developed a new synthetic strategy to construct Ln heterobimetallic complexes, which takes a hybrid approach using both thermodynamic and kinetic control over speciation. Individual reagents were designed using the ancillary ligands to fulfil two purposes: 1) to be kinetically inert to redistribution under reaction and spectroscopic conditions, and 2) to tune the coordination properties of the Ln to thermodynamically predispose binding to one of the two different sites of an asymmetric bridging ligand. By tailoring the reagents in this way to a bridging ligand with desirable redox activity (pd), we successfully incorporated such a ligand in Ln heteromultimetallic complexes for the first time.

The selective speciation of **3-LnLn'** is evidenced by NMR spectroscopy, by crystallography, and by PL spectroscopy. We were able to use the unique and characteristic PCS contributions of Ln^{3+} ions in different coordination sites to the chemical shifts of ^{1}H NMR resonances in **3-LnLn'**, which provided a useful analytical handle.

Sensitisation of Ln^{3+} PL in **3-LnLn'** was studied, where excitation of ancillary ligands could be used to selectively induce emission from one or both Ln^{3+} ions *via* complex and directional ET pathways which are of interest for optical and sensing purposes. Variations in the Stark sub-level splitting of Yb^{3+} PL emission caused by the different coordination environments of Yb^{3+} in **3-YbEu** and **3-DyYb** further support the binding site selectivity. Unusually, not only is emission observed in **1-Ln** and **3-LnLn'** from lanthanides which are directly coordinated by a radical ligand, but the radical ligand in both **1-Ln** and **3-LnLn'** coordinates *via* its open-shell semiquinone *O,O'* site, and that emission results after direct excitation of the radical ligand. Here, $pd^{\bullet-}$ is shown to sensitise PL from both Eu^{3+} and Yb^{3+}, providing an unusual example of participation of a doublet state in sensitisation of lanthanide PL.

We demonstrated our synthetic strategy's application in different combinations of Ln^{3+}, opening the possibility of a systematic study of the interactivity and cooperativity between Ln, as well as intentional design for applications in magneto-optics and quantum information science. Furthermore, the synthetic methodology we have described should be applicable to a wide range of both metal ions and asymmetric bridging ligands. This provides the opportunity to access new multimetallic systems featuring ionic and non-directionally bonding metals such as those in the *f*- and *s*-blocks and will allow the chemistry of such metals to be explored in new environments.

Supplementary information

Electronic supplementary information including further synthetic details, spectroscopy, and crystallographic characterisation information is available as a pdf. Crystallographic data for complexes **1-Yb**, **1-Dy**, **2-Eu**, **3-YbEu** and **3-DyYb** is available from the CCDC under deposition numbers 2295951-2295956.

References

1) Kretschmer, J., David, T., Dračínský, M., Socha, O., Jirak, D., Vít, M.*, et al.* Paramagnetic encoding of molecules. *Nat. Commun.* 2022, **13**(1)**:** 3179.
2) Kreidt, E., Leis, W., Seitz, M. Direct solid-phase synthesis of molecular heterooligonuclear lanthanoid-complexes. *Nat. Commun.* 2020, **11**(1)**:** 1346.
3) Bao, G., Wong, K.-L., Jin, D., Tanner, P.A. A stoichiometric terbium-europium dyad molecular thermometer: energy transfer properties. *Light Sci. Appl.* 2018, **7**(1)**:** 96.
4) Faulkner, S., Pope, S.J.A. Lanthanide-Sensitized Lanthanide Luminescence: Terbium-Sensitized Ytterbium Luminescence in a Trinuclear Complex. *J. Am. Chem. Soc.* 2003, **125**(35)**:** 10526-10527.
5) Thornton, M.E., Hemsworth, J., Hay, S., Parkinson, P., Faulkner, S., Natrajan, L.S. Heterometallic lanthanide complexes with site-specific binding that enable simultaneous visible and NIR-emission. *Front. Chem.* 2023, **11**.
6) Souri, N., Tian, P., Platas-Iglesias, C., Wong, K.-L., Nonat, A., Charbonnière, L.J. Upconverted Photosensitization of Tb Visible Emission by NIR Yb Excitation in Discrete Supramolecular Heteropolynuclear Complexes. *J. Am. Chem. Soc.* 2017, **139**(4)**:** 1456-1459.
7) Nonat, A., Bahamyirou, S., Lecointre, A., Przybilla, F., Mély, Y., Platas-Iglesias, C.*, et al.* Molecular Upconversion in Water in Heteropolynuclear Supramolecular Tb/Yb Assemblies. *J. Am. Chem. Soc.* 2019, **141**(4)**:** 1568-1576.
8) Abad Galán, L., Aguilà, D., Guyot, Y., Velasco, V., Roubeau, O., Teat, S.J.*, et al.* Accessing Lanthanide-to-Lanthanide Energy Transfer in a Family of Site-Resolved [LnIIILnIII'] Heterodimetallic Complexes. *Chem. Eur. J.* 2021, **27**(25)**:** 7288-7299.
9) Aguilà, D., Barrios, L.A., Velasco, V., Roubeau, O., Repollés, A., Alonso, P.J.*, et al.* Heterodimetallic [LnLn'] Lanthanide Complexes: Toward a Chemical Design of Two-Qubit Molecular Spin Quantum Gates. *J. Am. Chem. Soc.* 2014, **136**(40)**:** 14215-14222.
10) Maniaki, D., Garay-Ruiz, D., Barrios, L.A., Martins, D., Aguilà, D., Tuna, F.*, et al.* Unparalleled selectivity and electronic structure of heterometallic [LnLn'Ln] molecules as 3-qubit quantum gates. *Chem. Sci.* 2022, **13**(19)**:** 5574-5581.
11) Le Roy, J.J., Cremers, J., Thomlinson, I.A., Slota, M., Myers, W.K., Horton, P.H.*, et al.* Tailored homo- and hetero-lanthanide porphyrin dimers: a synthetic strategy for integrating multiple spintronic functionalities into a single molecule. *Chem. Sci.* 2018, **9**(45)**:** 8474-8481.
12) Jori, N., Falcone, M., Scopelliti, R., Mazzanti, M. Carbon Dioxide Reduction by Multimetallic Uranium(IV) Complexes Supported by Redox-Active Schiff Base Ligands. *Organometallics* 2020, **39**(9)**:** 1590-1601.

13) Kraft, S.J., Fanwick, P.E., Bart, S.C. Carbon–Carbon Reductive Elimination from Homoleptic Uranium(IV) Alkyls Induced by Redox-Active Ligands. *J. Am. Chem. Soc.* 2012, **134**(14)**:** 6160-6168.
14) Matson, E.M., Opperwall, S.R., Fanwick, P.E., Bart, S.C. "Oxidative Addition" of Halogens to Uranium(IV) Bis(amidophenolate) Complexes. *Inorg. Chem.* 2013, **52**(12)**:** 7295-7304.
15) Castro, L., So, Y.-M., Cho, C.-w., Lortz, R., Wong, K.-H., Wang, K.*, et al.* A Combined Experimental and Theoretical Study of the Versatile Reactivity of an Oxocerium(IV) Complex: Concerted Versus Reductive Addition. *Chem. Eur. J.* 2019, **25**(46)**:** 10834-10839.
16) Rinehart, J.D., Fang, M., Evans, W.J., Long, J.R. A N23– Radical-Bridged Terbium Complex Exhibiting Magnetic Hysteresis at 14 K. *J. Am. Chem. Soc.* 2011, **133**(36)**:** 14236-14239.
17) Gould Colin, A., Darago Lucy, E., Gonzalez Miguel, I., Demir, S., Long Jeffrey, R. A Trinuclear Radical-Bridged Lanthanide Single-Molecule Magnet. *Angew. Chem. Int. Ed.* 2017, **56**(34)**:** 10103-10107.
18) Sagawa, M., Mizoguchi, T., inventors; Sintered neodymium magnet and manufaturing method therefor patent EP2696355A1.01. 2014.
19) Goodwin, C.A.P., Ortu, F., Reta, D., Chilton, N.F., Mills, D.P. Molecular magnetic hysteresis at 60 kelvin in dysprosocenium. *Nature* 2017, **548:** 439.
20) Guo, F.-S., Day, B.M., Chen, Y.-C., Tong, M.-L., Mansikkamäki, A., Layfield, R.A. A Dysprosium Metallocene Single-Molecule Magnet Functioning at the Axial Limit. *Angew. Chem. Int. Ed.* 2017, **56**(38)**:** 11445-11449.
21) Bünzli, J.-C.G. Lanthanide Luminescence for Biomedical Analyses and Imaging. *Chem. Rev.* 2010, **110**(5)**:** 2729-2755.
22) Bünzli, J.-C.G., Piguet, C. Taking advantage of luminescent lanthanide ions. *Chem. Soc. Rev.* 2005, **34**(12)**:** 1048-1077.
23) Lu, Y., Zhao, J., Zhang, R., Liu, Y., Liu, D., Goldys, E.M.*, et al.* Tunable lifetime multiplexing using luminescent nanocrystals. *Nat. Photonics* 2014, **8**(1)**:** 32-36.
24) Diaz-Rodriguez, R.M., Gálico, D.A., Chartrand, D., Suturina, E.A., Murugesu, M. Toward Opto-Structural Correlation to Investigate Luminescence Thermometry in an Organometallic Eu(II) Complex. *J. Am. Chem. Soc.* 2022, **144**(2)**:** 912-921.
25) Fan, Y., Wang, P., Lu, Y., Wang, R., Zhou, L., Zheng, X.*, et al.* Lifetime-engineered NIR-II nanoparticles unlock multiplexed in vivo imaging. *Nat. Nanotechnol.* 2018, **13**(10)**:** 941-946.
26) Costes, J.P., Dahan, F., Dupuis, A., Lagrave, S., Laurent, J.P. Homo- (4f, 4f) and Heterodimetallic (4f, 4f') Complexes. The First Structurally Characterized Example of a Heterodimetallic (Yb, La) Complex (1'). Magnetic Properties of 1' and of a Homodinuclear (Gd, Gd) Analogue. *Inorg. Chem.* 1998, **37**(1)**:** 153-155.
27) André, N., Scopelliti, R., Hopfgartner, G., Piguet, C., Bünzli, J.-C.G. Discriminating between lanthanide ions: self-assembly of heterodimetallic triple-stranded helicates. *Chem. Commun.* 2002, **38**(3)**:** 214-215.
28) Sørensen, T.J., Faulkner, S. Multimetallic Lanthanide Complexes: Using Kinetic Control To Define Complex Multimetallic Arrays. *Acc. Chem. Res.* 2018, **51**(10)**:** 2493-2501.
29) Gross, T., Chevalier, F., Lindsey, J.S. Investigation of Rational Syntheses of Heteroleptic Porphyrinic Lanthanide (Europium, Cerium) Triple-Decker Sandwich Complexes. *Inorg. Chem.* 2001, **40**(18)**:** 4762-4774.
30) Hickson, J.R., Horsewill, S.J., Bamforth, C., McGuire, J., Wilson, C., Sproules, S.*, et al.* The modular synthesis of rare earth-transition metal heterobimetallic complexes utilizing a redox-active ligand. *Dalton Trans.* 2018, **47**(31)**:** 10692-10701.
31) Hickson, J.R., Horsewill, S.J., McGuire, J., Wilson, C., Sproules, S., Farnaby, J.H. The semiquinone radical anion of 1,10-phenanthroline-5,6-dione: synthesis and rare earth coordination chemistry. *Chem. Commun.* 2018, **54**(80)**:** 11284-11287.
32) Shavaleev, N.M., Moorcraft, L.P., Pope, S.J.A., Bell, Z.R., Faulkner, S., Ward, M.D. Sensitized Near-Infrared Emission from Complexes of YbIII, NdIII and ErIII by Energy-Transfer from Covalently Attached PtII-Based Antenna Units. *Chem. Eur. J.* 2003, **9**(21)**:** 5283-5291.
33) Shavaleev, N.M., Moorcraft, L.P., Pope, S.J.A., Bell, Z.R., Faulkner, S., Ward, M.D. Sensitised near-infrared emission from lanthanides using a covalently-attached Pt(ii) fragment as an antenna group. *Chem. Commun.* 2003, **39**(10)**:** 1134-1135.
34) Dunstan, M.A., Rousset, E., Boulon, M.-E., Gable, R.W., Sorace, L., Boskovic, C. Slow magnetisation relaxation in tetraoxolene-bridged rare earth complexes. *Dalton Trans.* 2017, **46**(40)**:** 13756-13767.
35) Zhang, P., Perfetti, M., Kern, M., Hallmen, P.P., Ungur, L., Lenz, S.*, et al.* Exchange coupling and single molecule magnetism in redox-active tetraoxolene-bridged dilanthanide complexes. *Chem. Sci.* 2018, **9**(5)**:** 1221-1230.
36) Chowdhury, T., Horsewill, S.J., Wilson, C., Farnaby, J.H. Heteroleptic lanthanide(III) complexes: synthetic utility and versatility of the unsubstituted bis-scorpionate ligand framework. *Aust. J. Chem.* 2022, **75**(9)**:** 660-675.
37) McGuire, J., Wilson, B., McAllister, J., Miras, H.N., Wilson, C., Sproules, S.*, et al.* Molecular and electronic structure of the dithiooxalato radical ligand stabilised by rare earth coordination. *Dalton Trans.* 2019, **48**(17)**:** 5491-5495.
38) Caneschi, A., Dei, A., Gatteschi, D., Sorace, L., Vostrikova, K. Antiferromagnetic Coupling in a Gadolinium(III) Semiquinonato Complex. *Angew. Chem. Int. Ed.* 2000, **39**(1)**:** 246-248.
39) Chowdhury, T., Evans, M.J., Coles, M.P., Bailey, A.G., Peveler, W.J., Wilson, C.*, et al.* Reduction chemistry yields stable and soluble divalent lanthanide tris(pyrazolyl)borate complexes. *Chem. Commun.* 2023, **59**(15)**:** 2134-2137.
40) Dai, J.-W., Li, Z.-Y., Sato, O. 1,10-Phenanthroline-5,6-dione ethanol monosolvate. *Acta Cryst. Sect. E* 2014, **70**(5)**:** o573.
41) Gorgon, S., Lv, K., Grüne, J., Drummond, B.H., Myers, W.K., Londi, G.*, et al.* Reversible spin-optical interface in luminescent organic radicals. *Nature* 2023, **620**(7974)**:** 538-544.
42) Jiang, W., Wu, S., Xu, D., Tu, L., Xie, Y., Pasqués-Gramage, P.*, et al.* Stable Xanthene Radicals and Their Heavy Chalcogen Analogues Showing Tunable Doublet Emission from Green to Near-infrared. *Angew. Chem. Int. Ed.* 2024, **n/a**(n/a)**:** e202418762.
43) Horsewill, S.J. Modular Synthesis of Lanthanide Heterobimetallic Complexes. Doctor of Philosophy (PhD) thesis, University of Glasgow, 2021.